Quantum microarchitecture

Yipeng Huang

Rutgers University

November 30, 2022

Table of contents

Essential hardware components of a quantum computer

Host processor plane

Control processor plane

digital processing, non-deterministic timing

Control and measurement plane

analog processing, deterministic timing

Quantum data plane

[National Academies of Sciences, Engineering, and Medicine, 2019, Chapter 5]

TU Delft control and measurement processors

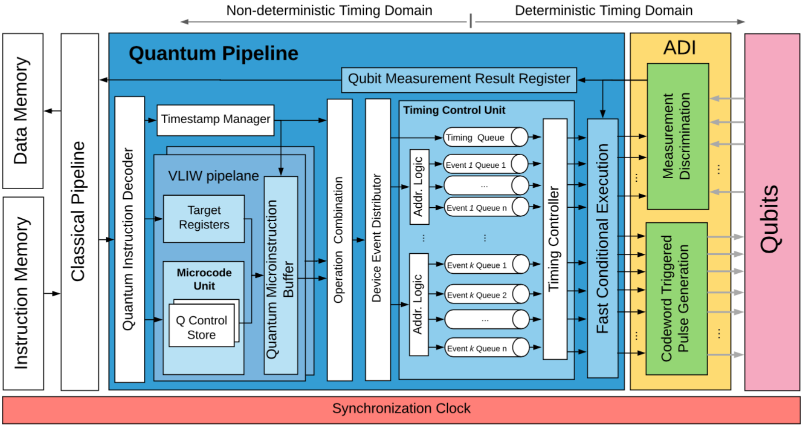

Fig. 9. Quantum microarchitecture implementing the instantiated eQASM for the seven-qubit superconducting quantum processor.

Figure: Credit: [Fu et al., 2019]

This is an example for superconducting qubits.

Table of contents

DiVincenzo's criteria

The central challenge

Keeping qubits weakly coupled to external decoherence forces, while keeping them strongly coupled to each other.

Examples

The requirements are often conflicting: single nuclear spin can remain in a superposition state for days, but because it couples so weakly with the world, control and measurement is hard.

DiVincenzo's criteria

1. A scalable physical system with well characterized qubits
2. The ability to initialize the state of the qubits to a simple fiducial state, such as $|000\ldots\rangle$
3. Long relevant decoherence times, much longer than the gate operation time
4. A "universal" set of quantum gates
5. A qubit-specific measurement capability
6. The ability to interconvert stationary and flying qubits
7. The ability to transmit faithfully flying qubits between specified locations

Table of contents

Trapped ion quantum computers

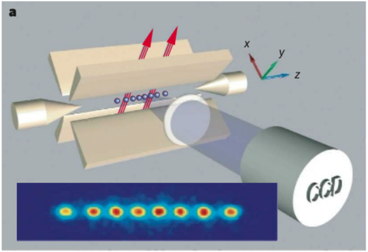

FIG. 2: Schematic of ion trap apparatus. Electric potentials are applied to appropriate electrodes in order to confine a 1-D crystal of individual atomic ions. Lasers affect coherent spin-dependent forces to the ions that can entangle their internal qubit levels through their Coulomb-coupled motion. Resonant lasers can also cause spin-dependent flourescence for the efficient detection of the trapped ion qubit states. The inset shows a collection of atomic Ca^+ ions fluorescing (courtesy R. Blatt, University of Innsbruck).

Figure: Credit: [Ladd et al., 2010]

Strengths

Long coherence, high inter-connectivity

Weaknesses

Rely on multiple interacting technologies, relatively slow (1–100μS) gate operation times

Examples

Research groups: University of Maryland, IonQ, Honeywell

DiVincenzo's criteria

1. A scalable physical system with well characterized qubits
2. The ability to initialize the state of the qubits to a simple fiducial state, such as $|000\ldots\rangle$
3. Long relevant decoherence times, much longer than the gate operation time
4. A "universal" set of quantum gates
5. A qubit-specific measurement capability
6. The ability to interconvert stationary and flying qubits
7. The ability to transmit faithfully flying qubits between specified locations

Ion traps: A scalable physical system with well characterized qubits

Optical qubits

Ground electronic state and a metastable excited electronic state. Large gap, higher frequency, optical laser for control.

Hyperfine qubits

Pair of energy states resulting from nucleus with non-zero spin with smaller energy difference. Small gap, lower frequency, microwave sources for control.

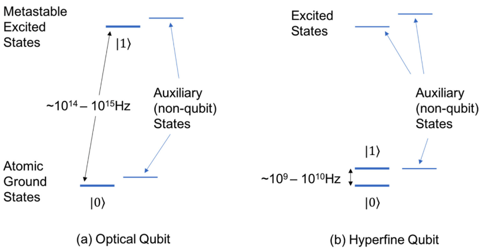

FIGURE B.2 Qubits in an atomic ion. (a) An optical qubit consists of one of the atomic ground states and one of the metastable excited states, separated by ~10^{14} to 10^{15} Hz. (b) A hyperfine qubit consists of two of the ground states, separated by ~10^{9} to 10^{10} Hz. Usually some excited states are used to support qubit manipulation operations. In both cases, there are other (auxiliary) states in the ground, excited, and metastable excited states than those chosen to represent the qubit.

Figure:
Credit: [National Academies of Sciences, Engi

Ion traps: A scalable physical system with well characterized qubits

Optical qubits

Ground electronic state and a metastable excited electronic state. Large gap, higher frequency, optical laser for control.

Hyperfine qubits

Pair of energy states resulting from nucleus with non-zero spin with smaller energy difference. Small gap, lower frequency, microwave sources for control.

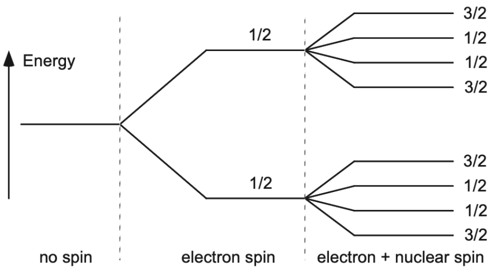

Figure:
Credit: [Nielsen and Chuang, 2011]

Ion traps: Long relevant decoherence times, much longer than the gate operation time

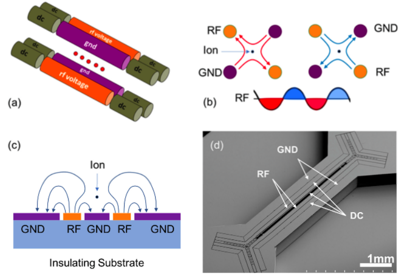

FIGURE B.1 Operating principle of RF Paul trap. (a) An example of a traditional RF Paul trap using four rods. Two rods in the diagonal serve as RF grounds, while an RF voltage is applied to the remaining two. This geometry creates a quadrupole electric field profile in the plane perpendicular to the axis of the rods and forms a one-dimensional (1D) linear trapping potential, where a chain of ions can be readily trapped. SOURCE: Image from D. Hayes, Ph.D. thesis, University of Maryland, 2012. (b) During the negative cycle of the RF voltage (red arrows), the positively charged ion is pushed away from the ground electrodes toward the RF electrodes, while during the positive cycle of the RF voltage (blue arrows), the ions are pushed in the opposite direction. If the frequency of the RF voltage is much higher than the natural motional frequency of the ion (called the "secular frequency"), then the ions feel confining potential where the electric field forms a quadrupole null ("zero-field region"). (c) A linear trapping potential can be created by electrodes fabricated on a planar surface of a substrate. The cross-sectional view of the electric field forms the quadrupole null, and a linear trap is formed above the surface of the trap. (d) An example of a microfabricated surface trap, designed to provide adequate optical access to the ions trapped above the surface of the trapping electrodes. SOURCE: Image courtesy of Sandia National Labs, 2015.

Figure: Credit: NAP.

High vacuum

Radio frequency Paul trap

Like a rotating saddle. RF at 20–200 MHz. Voltage amplitudes 30–400 V.

Direct current axial trap

DC axial trap 0-30V

Ion traps: Long relevant decoherence times, much longer than the gate operation time

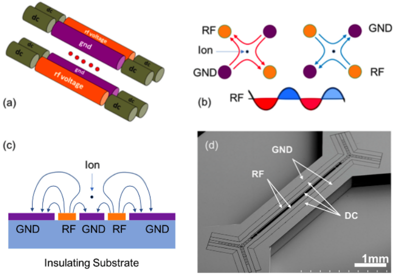

FIGURE B.1 Operating principle of RF Paul trap. (a) An example of a traditional RF Paul trap using four rods. Two rods in the diagonal serve as RF grounds, while an RF voltage is applied to the remaining two. This geometry creates a quadrupole electric field profile in the plane perpendicular to the axis of the rods and forms a one-dimensional (1D) linear trapping potential, where a chain of ions can be readily trapped. SOURCE: Image from D. Hayes, Ph.D. thesis, University of Maryland, 2012. (b) During the negative cycle of the RF voltage (red arrows), the positively charged ion is pushed away from the ground electrodes toward the RF electrodes, while during the positive cycle of the RF voltage (blue arrows), the ions are pushed in the opposite direction. If the frequency of the RF voltage is much higher than the natural motional frequency of the ion (called the "secular frequency"), then the ions feel confining potential where the electric field forms a quadrupole null ("zero-field region"). (c) A linear trapping potential can be created by electrodes fabricated on a planar surface of a substrate. The cross-sectional view of the electric field forms the quadrupole null, and a linear trap is formed above the surface of the trap. (d) An example of a microfabricated surface trap, designed to provide adequate optical access to the ions trapped above the surface of the trapping electrodes. SOURCE: Image courtesy of Sandia National Labs, 2015.

Figure: Credit: NAP.

An artificial 1 dimensional crystal

Once ions are settled in trap, confined in two dimensions with more freedom to move axially. They repel and interact with each other due to Coulomb repulsion.

Ion traps: The ability to initialize the state of the qubits to a simple fiducial state, such as $|000\ldots\rangle$

Cooling the ions down to ground state

Continuous wave lasers carry away momentum from system.

Ion traps: A "universal" set of quantum gates

Coherent qubit control system

Single qubit gates

Rabi oscillations between the two qubit levels with resonant laser pulses.

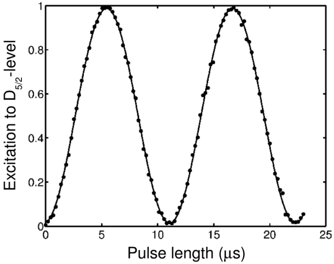

Fig. 6. Rabi oscillations of a single Ca^+ ion. Each dot represents 1000 experiments, each consisting of initialization, application of laser light on the qubit transition and state detection.

Figure: Credit: [Häffner et al., 2008]

Fig. 16.1 Rabi oscillations

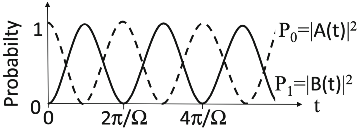

Figure: Credit: [LaPierre, 2021]

Ion traps: A "universal" set of quantum gates

Two qubit gates

1. State-dependent force.
2. Ignacio Cirac and Peter Zoller two qubit gate in 1995.
3. Molmer-Sorensen gate.
4. Global entangling gate, or pair-wise control signals.
5. 2–5% error rates for two-qubit gates.

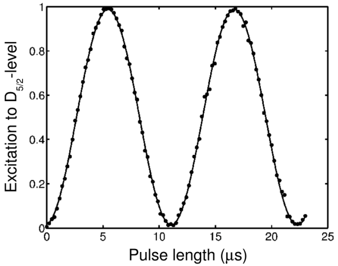

Fig. 6. Rabi oscillations of a single Ca^{+} ion. Each dot represents 1000 experiments, each consisting of initialization, application of laser light on the qubit transition and state detection.

Figure: Credit: [Häffner et al., 2008]

Ion traps: A qubit-specific measurement capability

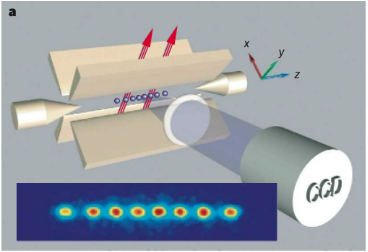

FIG. 2: Schematic of ion trap apparatus. Electric potentials are applied to appropriate electrodes in order to confine a 1-D crystal of individual atomic ions. Lasers affect coherent spin-dependent forces to the ions that can entangle their internal qubit levels through their Coulomb-coupled motion. Resonant lasers can also cause spin-dependent flourescence for the efficient detection of the trapped ion qubit states. The inset shows a collection of atomic Ca^+ ions fluorescing (courtesy R. Blatt, University of Innsbruck).

Figure: Credit: [Ladd et al., 2010]

1. Continuous wave lasers for read out illumination.
2. Mössbauer effect / state-dependent fluorescence.
3. Photon detectors.

Ion traps: The ability to interconvert stationary and flying qubits

1. Each trap may scale to over 50 qubits.
2. Proposals to couple distant traps via photonics or via entangled ions.

Ion traps: The ability to transmit faithfully flying qubits between specified locations

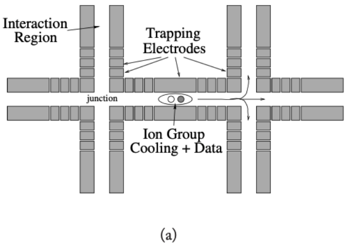

Figure 4.2: (a) The physical structure of an ion-trap quantum computer. An optimistic size of the trapping electrodes is in the order of tens of micrometers [193]. The data ion is kept together with a cooling ion and cooled before and after each movement step or logic gate. The ion-group can move to any of the 6 adjacent trapping regions for interaction with another ion-group.(b) A two-qubit gate sequence where the ion-group in the top left junction moves to the middle for a two-qubit gate. The gate is implemented with an external laser beam acting on the two ion-groups.

Figure: Ion shuttling. Credit: [Metodi and Chong, 2006]

Table of contents

Superconducting quantum computers

Strengths

Solid state, lithographically defined (single mask, single metal layer), relatively fast (10–100nS) gate operation times

Weaknesses

Variability, cryogenic

Examples

Research groups: IBM, Google (Bristlecone, Sycamore), Rigetti

DiVincenzo's criteria

1. A scalable physical system with well characterized qubits
2. The ability to initialize the state of the qubits to a simple fiducial state, such as $|000\ldots\rangle$
3. Long relevant decoherence times, much longer than the gate operation time
4. A "universal" set of quantum gates
5. A qubit-specific measurement capability
6. The ability to interconvert stationary and flying qubits
7. The ability to transmit faithfully flying qubits between specified locations

Superconductors: A scalable physical system with well characterized qubits

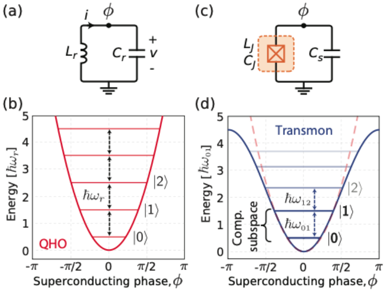

FIG. 1. **(a)** Circuit for a parallel LC-oscillator (quantum harmonic oscillator, QHO), with inductance L in parallel with capacitance, C. The superconducting phase on the island is denoted ϕ, referencing ground as zero. **(b)** Energy potential for the QHO, where energy levels are equidistantly spaced $\hbar\omega_r$ apart. **(c)** Josephson qubit circuit, where the nonlinear inductance L_J (represented with the Josephson-subcircuit in the dashed orange box) is shunted by a capacitance, C_s. **(d)** The Josephson inductance reshapes the quadratic energy potential (dashed red) into sinusoidal (solid blue), which yields non-equidistant energy levels. This allows us to isolate the two lowest energy levels $|0\rangle$ and $|1\rangle$, forming a computational subspace with an energy separation $\hbar\omega_{01}$, which is different than $\hbar\omega_{12}$.

Linear resonator

Superconducting resonator

$H = \frac{\Phi^2}{2L} + \frac{Q^2}{2C}$

$H = \hbar\omega_0(n + \frac{1}{2})$

$w_0 = \frac{1}{\sqrt{LC}}$

C (capacitance acts as mass

L (inductance) acts as spring

[Devoret et al., 2004]

Superconductors: A scalable physical system with well characterized qubits

Nonlinear resonator

1. Nonlinear inductor: Josephson junction.
2. Insulator sandwiched between two superconductors.
3. Al-AlOx-Al.
4. Josephson junction introduces nonlinearity.
5. electrons pair up to form Cooper pairs, which allow them to tunnel across the insulator in discrete quanta.

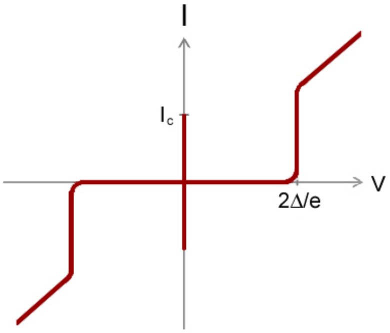

Figure: Credit: wikimedia.org

Superconductors: A scalable physical system with well characterized qubits

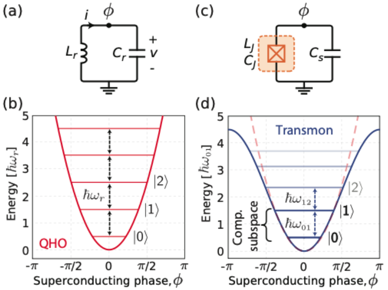

FIG. 1. **(a)** Circuit for a parallel LC-oscillator (quantum harmonic oscillator, QHO), with inductance L in parallel with capacitance, C. The superconducting phase on the island is denoted ϕ, referencing ground as zero. **(b)** Energy potential for the QHO, where energy levels are equidistantly spaced $\hbar\omega_r$ apart. **(c)** Josephson qubit circuit, where the nonlinear inductance L_J (represented with the Josephson-subcircuit in the dashed orange box) is shunted by a capacitance, C_s. **(d)** The Josephson inductance reshapes the quadratic energy potential (dashed red) into sinusoidal (solid blue), which yields non-equidistant energy levels. This allows us to isolate the two lowest energy levels $|0\rangle$ and $|1\rangle$, forming a computational subspace with an energy separation $\hbar\omega_{01}$, which is different than $\hbar\omega_{12}$.

Artificial atoms with atom-like spectra

Anharmonicity describes the difference between $\hbar\omega_{01}$ and $\hbar\omega_{12}$.

Superconductors: Long relevant decoherence times, much longer than the gate operation time

Superconductors and cryogenic temperatures needed for qubit coherence

1. Superconductivity eliminates heat dissipation with current.
2. Cryogenic temperatures eliminate state transitions due to thermal excitation (5GHz microwave corresponds to thermal energy of 250mK).
3. Cryogenic temperatures also needed for superconductivity (for aluminium, $T_c = 1.2$K).

Superconductors: Long relevant decoherence times, much longer than the gate operation time

Dilution refrigerator

1. Dry refrigerator cools to 50K and 3K. Here, thermal budget is 1W.
2. Liquid helium cools to 700mK, 50mK, 10mK. Here, thermal budget is 30μW–1mW.

Cryogenic signal processing stage-by-stage

1. Thermally resistive will necessarily imply electrically lossy.
2. Filter out the noise.
3. Attenuate to send to next stage.

Takes 2 days to cool down to operating temperature.

Superconductors: A "universal" set of quantum gates

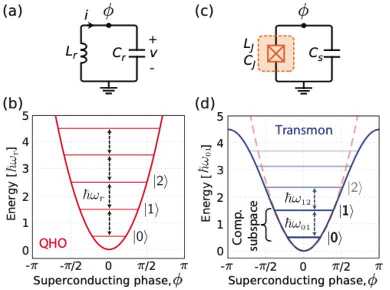

FIG. 1. **(a)** Circuit for a parallel LC-oscillator (quantum harmonic oscillator, QHO), with inductance L in parallel with capacitance, C. The superconducting phase on the island is denoted ϕ, referencing ground as zero. **(b)** Energy potential for the QHO, where energy levels are equidistantly spaced $\hbar\omega_r$ apart. **(c)** Josephson qubit circuit, where the nonlinear inductance L_J (represented with the Josephson-subcircuit in the dashed orange box) is shunted by a capacitance, C_s. **(d)** The Josephson inductance reshapes the quadratic energy potential (dashed red) into sinusoidal (solid blue), which yields non-equidistant energy levels. This allows us to isolate the two lowest energy levels $|0\rangle$ and $|1\rangle$, forming a computational subspace with an energy separation $\hbar\omega_{01}$, which is different than $\hbar\omega_{12}$.

Figure: Credit: [Krantz et al., 2019]

Single qubit gates

1. JJ reshapes the parabolic energy well so that gap between lower energy levels is wider.
2. Creates a f_{01} transition frequency.
3. Then you can change the state (I,V) by injecting microwaves at the right frequency.
4. $\approx$ 5GHz microwaves stimulate transition, with standard deviation $\sigma \approx$ 150MHz.

Superconductors: A "universal" set of quantum gates

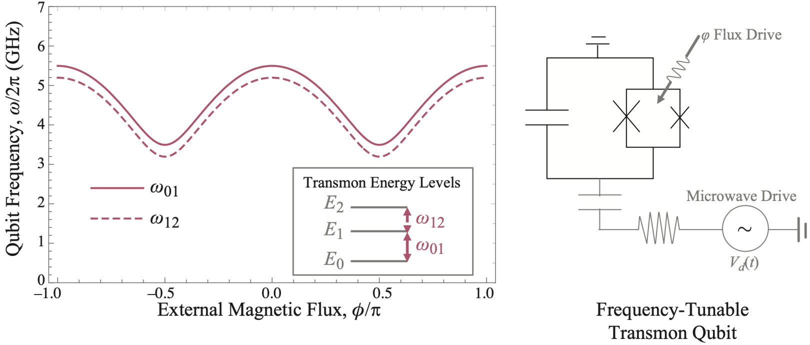

Figure 2.12: **Left:** Qubit frequencies as a function of external magnetic flux. The first three levels of the transmon, ω_{01} and ω_{12}, are plotted. **Right:** Circuit diagram for a frequency-tunable (asymmetric) transmon qubit (highlighted in black), consisting of a capacitor and two asymmetric Josephson junctions. Highlighted in gray are two control lines: the external magnetic flux control φ and microwave voltage drive line $V_d(t)$ for each transmon qubit.

Figure: Credit: [Ding and Chong, 2020, Chapter 2.4.2]

Superconductors: A “universal” set of quantum gates

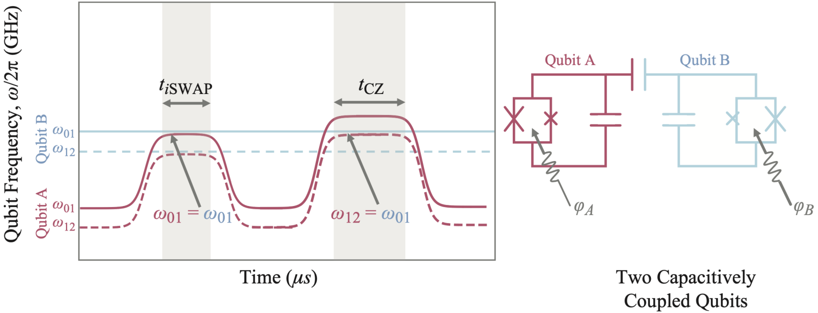

Figure 2.13: Two-qubit interactions for two capacitively coupled transmons. **Left:** Two-qubit gates are implemented with resonance of qubit frequencies. Shown here are how qubit frequencies are tuned for *i*SWAP gate and CZ gate. **Right:** Circuit diagram of two capacitively coupled transmon qubits.

Figure: Credit: [Ding and Chong, 2020, Chapter 2.4.2]

Superconductors: A "universal" set of quantum gates

Native two qubit gates

1. iSWAP
2. CZ
3. CR

Frequency allocation

1. Single junction nontunable
2. Two-junction tunable

Examples

OpenPulse.

Superconductors: A qubit-specific measurement capability

- Dispersive readout
- State-dependent frequency shift of a resonator coupled to each qubit [Ding and Chong, 2020, Chapter 2.4.2]

Superconducting quantum computers

Strengths

Solid state, lithographically defined (single mask, single metal layer), relatively fast (10–100nS) gate operation times

Weaknesses

Variability, cryogenic, CMOS processes for superconducting circuit and peripheral circuitry not compatible, limited physical volume in cryostat

Examples

Research groups: IBM, Google (Bristlecone, Sycamore), Rigetti

Table of contents

Other technologies

Trapped ions and superconductors are currently the only technologies with full-stack integration.

In fact, it is quite remarkable that both are at comparable maturity level, given the wildly different technologies involved.

Outside of TI and SC, other technologies are demonstrating single and two qubit gates.

Other technologies

Atomic, molecular, and optical physics

Trapped optical ion, trapped (hyperfine) microwave/RF ion, trapped neutral atoms, liquid nuclear magnetic resonance.

Solid-state

GaAs quantum dot, optically active defects, diamond defects, nitrogen vacancy centers, superconducting phase/charge/flux qubit.

All are in infancy.

Hard to bet on long term winner.

Other technologies

	Type of Matter Qubit	Coherence			Benchmarking	
		$\omega_0/2\pi$	T_2	Q	1 qbit	2 qbit
AMO	Trapped Optical Ion[22,23] ($^{40}Ca^+$)	400 THz	1 ms	10^{12}	0.1%	0.7%*
AMO	Trapped Microwave Ion[24–26] ($^{9}Be^+$)	300 MHz	10 sec	10^{10}	0.48%†	3%
AMO	Trapped Neutral Atoms[27] (^{87}Rb)	7 GHz	3 sec	10^{11}	5%	
AMO	Liquid Molecule Nuclear Spins[28]	500 MHz	2 sec	10^{9}	0.01%†	0.47%†
Solid-State	e^- Spin in GaAs Quantum Dot[29–31]	10 GHz	3 μs	10^{5}	5%	
Solid-State	e^- Spins Bound to ^{31}P:^{28}Si[32,33]	10 GHz	60 ms	10^{9}	5%	10%
Solid-State	Nuclear Spins in Si[34]	60 MHz	25 sec	10^{9}	5%	
Solid-State	NV^- Center in Diamond[35–37]	3 GHz	2 ms	10^{7}	2%	5%
Solid-State	Superconducting Phase Qubit[38–40]	10 GHz	350 ns	10^{4}	2%*	24%*
Solid-State	Superconducting Charge Qubit[41–43]	10 GHz	2 μs	10^{5}	1.1%†	10%*
Solid-State	Superconducting Flux Qubit[44,45]	10 GHz	4 μs	10^{5}	3%	60%

Table comparing the current performance of various matter qubits. The approximate resonant frequency of each qubit is listed as $\omega_0/2\pi$; this is not necessarily the speed of operation, but sets a limit for defining the phase of a single qubit. Therefore, $Q = \omega_0 T_2$ is a very rough quality factor. Benchmarking values show approximate error rates for single or multi-qubit gates. Values marked with * are found by state tomography, and give the departure of the fidelity from 100%. Values marked with † are found with randomized benchmarking. Other values are rough experimental gate error estimates.

Figure: Credit: [Ladd et al., 2010]

Other technologies

System	τ_Q	τ_{op}	$n_{op} = \lambda^{-1}$
Nuclear spin	$10^{-2} - 10^{8}$	$10^{-3} - 10^{-6}$	$10^{5} - 10^{14}$
Electron spin	10^{-3}	10^{-7}	10^{4}
Ion trap (In^+)	10^{-1}	10^{-14}	10^{13}
Electron – Au	10^{-8}	10^{-14}	10^{6}
Electron – GaAs	10^{-10}	10^{-13}	10^{3}
Quantum dot	10^{-6}	10^{-9}	10^{3}
Optical cavity	10^{-5}	10^{-14}	10^{9}
Microwave cavity	10^{0}	10^{-4}	10^{4}

Figure 7.1. Crude estimates for decoherence times τ_Q (seconds), operation times τ_{op} (seconds), and maximum number of operations $n_{op} = \lambda^{-1} = \tau_Q/\tau_{op}$ for various candidate physical realizations of interacting systems of quantum bits. Despite the number of entries in this table, only three fundamentally different qubit representations are given: spin, charge, and photon. The ion trap utilizes either fine or hyperfine transitions of a trapped atom (Section 7.6), which correspond to electron and nuclear spin flips. The estimates for electrons in gold and GaAs, and in quantum dots are given for a charge representation, with an electrode or some confined area either containing an electron or not. In optical and microwave cavities, photons (of frequencies from gigahertz to hundreds of terahertz) populating different modes of the cavities represent the qubit. Take these estimates with a grain of salt: they are only meant to give some perspective on the wide range of possibilities.

Figure: Credit: [Nielsen and Chuang, 2011]

Other technologies

Technology	Coherence Time (s)	1-Qubit Gate Latency (s)	2-Qubit Gate Latency (s)	1-Qubit Gate Fidelity (%)	2-Qubit Gate Fidelity (%)	Mobile
Ion Trap	0.2 [165] - 0.5 [169]	1.6e-6 [166] - 2e-5 [169]	5.4e-7 [166] - 2.5e-4 [169]	99.1 [169] - 99.9999 [168]	97 [169] - 99.9 [165]	YES
Superconductors	7.0e-6 [182] - 9.5e-5 [178]	2.0e-8 [62, 177, 180] - 1.30e-7 [78, 169]	3.0e-8 [182] - 2.5e-7 [78, 169]	98 [179] - 99.92 [177]	96.5 [78, 169] - 99.4 [177]	NO
Solid State Nuclear spin	0.6 [183]	1.12e-4 [184] - 1.5e-4 [183]	1.2e-4 [185]*	99.6 - [184] - 99.95 [183]	89 [186] - 96 [185]*	NO
Solid State Electron spin	1e-3 [3]	3.0e-6 [183] - 2.3e-5 [184]	1.2e-4 [185]*	99.4 [184] - 99.93 [183]	89 [186] - 96 [185]*	NO
Quantum Dot	1e-6 [3, 187] - 4e-4 [173]	1e-9 [3] - 2e-8 [171]	1e-7 [174]	98.6 [171] - 99.9 [172]	90 [171]	NO
NMR	16.7 [158]	2.5e-4 [158] - 1e-3 [24]	2.7e-3 [158] - 1.0e-2 [24]	98.74 [24] - 99.60 [158]	98.23 [24] - 98.77 [158]	NO

Table 1. Metrics for various quantum technologies. * Nuclear/Electron Hybrid

Figure: Credit: [Resch and Karpuzcu, 2019]

Primary sources

- [National Academies of Sciences, Engineering, and Medicine, 201
  Chapter 5, Appendix B, Appendix C]
- [DiVincenzo, 2000]
- [Nielsen and Chuang, 2011, Chapter 1.5]
- [Nielsen and Chuang, 2011, Chapter 7]
- [Marinescu, 2011, Chapter 6]

Devoret, M. H., Wallraff, A., and Martinis, J. M. (2004).
Superconducting qubits: A short review.
arXiv preprint cond-mat/0411174.

Ding, Y. and Chong, F. T. (2020).
Quantum computer systems: Research for noisy intermediate-scale quantum computers.
Synthesis Lectures on Computer Architecture, 15(2):1–227.

DiVincenzo, D. P. (2000).
The physical implementation of quantum computation.
Fortschritte der Physik: Progress of Physics, 48(9-11):771–783.

Fu, X., Riesebos, L., Rol, M. A., van Straten, J., van Someren, J., Khammassi, N., Ashraf, I., Vermeulen, R. F. L., Newsum, V., Loh, K. K. L., de Sterke, J. C., Vlothuizen, W. J., Schouten, R. N., Almudever, C. G., DiCarlo, L., and Bertels, K. (2019).
eqasm: An executable quantum instruction set architecture.
In *2019 IEEE International Symposium on High Performance Computer Architecture (HPCA)*, pages 224–237.

Häffner, H., Roos, C. F., and Blatt, R. (2008).
Quantum computing with trapped ions.
Physics reports, 469(4):155–203.

Krantz, P., Kjaergaard, M., Yan, F., Orlando, T. P., Gustavsson, S., and Oliver, W. D. (2019).
A quantum engineer's guide to superconducting qubits.
Applied Physics Reviews, 6(2):021318.

Ladd, T. D., Jelezko, F., Laflamme, R., Nakamura, Y., Monroe, C., and O'Brien, J. L. (2010).
Quantum computers.
Nature, 464(7285):45–53.

LaPierre, R. (2021).
Introduction to Quantum Computing.
The Materials Research Society Series. Springer International Publishing.

Marinescu, D. C. (2011).
Classical and quantum information.
Academic Press.

Metodi, T. S. and Chong, F. T. (2006).
Quantum Computing for Computer Architects (Synthesis Lectures on Computer Architecture).
Morgan and Claypool Publishers.

National Academies of Sciences, Engineering, and Medicine (2019).
Quantum Computing: Progress and Prospects.
The National Academies Press, Washington, DC.

Nielsen, M. A. and Chuang, I. L. (2011).
Quantum Computation and Quantum Information: 10th Anniversary Edition.
Cambridge University Press, USA, 10th edition.

Resch, S. and Karpuzcu, U. R. (2019).
Quantum computing: An overview across the system stack.